Controlling the dimensionality of charge transport in organic thin-film transistors

Ari Laiho, Lars Herlogsson, Robert Forchheimer, Xavier Crispin and Magnus Berggren

Original Publication:

Ari Laiho, Lars Herlogsson, Robert Forchheimer, Xavier Crispin and Magnus Berggren, Controlling the dimensionality of charge transport in organic thin-film transistors, 2011, Proceedings of the National Academy of Sciences of the United States of America, (108), 37, 15069-15073.
http://dx.doi.org/10.1073/pnas.1107063108

Controlling the dimensionality of charge transport in organic thin-film transistors

Ari Laiho [a], **Lars Herlogsson** [a], **Robert Forchheimer** [b], **Xavier Crispin** [a], **and Magnus Berggren** [a]

[a]Linköping University, Department of Science and Technology, Organic Electronics, SE-601 74 Norrköping, Sweden, and [b]Linköping University, Department of Electrical Engineering, SE-581 83 Linköping, Sweden

Published in the Proceedings of the National Academy of Sciences of the United States of America, www.pnas.org/cgi/doi/10.1073/pnas.1107063108

Electrolyte-gated organic thin-film transistors (OTFTs) can offer a feasible platform for future flexible, large-area and low-cost electronic applications. These transistors can be divided into two groups on the basis of their operation mechanism; i) field-effect transistors that switch fast but carry much less current than ii) the electrochemical transistors which, on the contrary, switch slowly. An attractive approach would be to combine the benefits of the field-effect and the electrochemical transistors into one transistor that would both switch fast and carry high current densities. Here we report the development of a polyelectrolyte-gated OTFT based on conjugated polyelectrolytes and we demonstrate that the OTFTs can be controllably operated either in the field-effect or the electrochemical regime. Moreover, we show that the extent of electrochemical doping can be restricted to a few monolayers of the conjugated polyelectrolyte film which allows both high current densities and fast switching speeds at the same time. We propose an operation mechanism based on self-doping of the conjugated polyelectrolyte backbone by its ionic side groups.

conjugated polyelectrolyte | conducting polymers | thin-film transistor | organic electronics

Correspondence should be addressed to magnus.berggren@itn.liu.se.

Incorporation of electronics into paper, plastic and other flexible, lightweight, thin and low-cost substrates can enable realization of a multitude of large-area electronic applications such as e-textiles, e-paper, lighting, photovoltaics and sensors. [1] In the field of organic electronics, considerable effort has been devoted to study organic thin-film transistors (OTFTs) which are regarded as the central components in each of the above mentioned applications. [2] OTFTs must meet a wide range of specifications to provide a feasible technology platform; they must be solution processable, operate at low voltages, consume only little power and they should also switch fast to enable fast signal processing. A promising solution to this problem is to use electrolytes as the gate "insulator" material. [3–6] Upon applying a gate potential, electrolytes can rapidly form electric double layers near the electrolyte-semiconductor interface which gives rise to high switching speeds, high electric fields and high charge carrier densities already at relatively low voltages. Polymer electrolytes and polyelectrolytes in particular are ideal due to their additional film-forming characteristics and ease of processing from solutions. More recently, a question on the operating mechanism of electrolyte-gated OTFTs has sparked a lively discussion as to whether the gating is purely field-induced or electrochemical. [7–9] In the former case, ions of the electrolyte migrate close to the semiconductor interface while charge carriers of opposite charge accumulate on the semiconductor side. The latter mechanism, on the other hand, is typically characterized by mass transport of ions across the electric double layer and involves electrochemical doping of the semiconductor bulk. Even if identification of the mechanism can be ambiguous, absorption [7, 10], Fourier transform [8] and impedance spectroscopy [11] as well as signatures in the electrical characteristics [12] have been used as evidences to judge the mode of operation. Electrochemical doping is most often (but not always) undesirable due to its deteriorating effect on the transistor performance such as considerably slower switching speed and large hysteresis in the electrical characteristics. [13] Therefore, several different techniques have been suggested to avoid electrochemical doping in electrolyte-gated OTFTs and include the use of highly crystalline semiconductors, immobile polyanions [13] and blocking layers between the semiconductor and the electrolyte [14]. Despite this drawback, electrochemical transistors have proven particularly useful for e.g. electrochromic displays which require high current densities to switch a pixel. [15, 16] An attractive approach is to combine the advantages of both field-effect and electrochemical transistors into one transistor that would both switch fast and carry a high current density.

In this article, we develop polyelectrolyte-gated OTFTs based on a carboxyl-functionalized poly(3-hexylthiophene) (P3CPT, Fig 1*B*). P3CPT belongs to a group of conjugated polyelectrolytes whose intriguing properties stem from the combination of a hydrophobic π-conjugated backbone with the physicochemical properties of a hydrophilic ionic side group. [17] Previously, this class of polymers has been used in organic photovoltaics [18], as gate dielectric material in transistors [19] or to improve the electrical contacts between electrodes and another semiconducting material. [20] Bao and coworkers demonstrated the use of carboxyl-functionalized polyalkylthiophenes in field-effect transistors [21] but the transistors showed only poor electrical and structural characteristics most probably due to the short alkyl spacer [18] and the low dielectric constant of the gate insulator. Our hypothesis is that the dual nature of the conjugated polyelectrolyte can allow bulk transport in an OTFT as the polarons in the conjugated backbone can be stabilized by the neighboring ionic side groups throughout the bulk of the semiconductor layer. Here, we first distinguish between the different operational regimes and compare the transistor characteristics of the P3CPT based transistor to its well-studied unmodified precursor poly(3-hexylthiophene) (P3HT, Fig. 1*B*). We show that polyelectrolyte-gated OTFTs comprising P3CPT operate either in the field-effect (Regime I in Fig. 1*A*) or electrochemical regime, depending on the applied gate voltage. Furthermore, we report two distinct switching processes in the electrochemical regime, which are attributed to *fast interfacial* and *slow bulk* electrochemical doping, respectively (Regime II and III in Fig. 1*A*). An operation mechanism based on self-doping of the conjugated backbone by the ionic side groups is proposed.

Results and Discussion

The chemical structures of the two conjugated polymers used in this study are shown in Fig. 1*B*. They differ with respect to the terminal group of the side chain of the polymer; either a methyl (-CH_3) or a carboxyl group (-COOH). As an example, the hydrophobic alkyl side chains of P3HT give rise to a water contact angle of 105° on a P3HT thin film whereas on a P3CPT film, water droplets show a considerably lower contact angle of 49° due to the hydrophilic carboxyl groups of P3CPT (Fig. 1*D* and *E*). The hydrophobicity of P3HT

Publication footnotes

A.L., L.H., X.C., and M.B. designed research; A.L. performed research, R.F. contributed new reagents/analytic tools; A.L. analyzed data; and A.L., L.H., R.F., X.C., and M.B. wrote the paper.

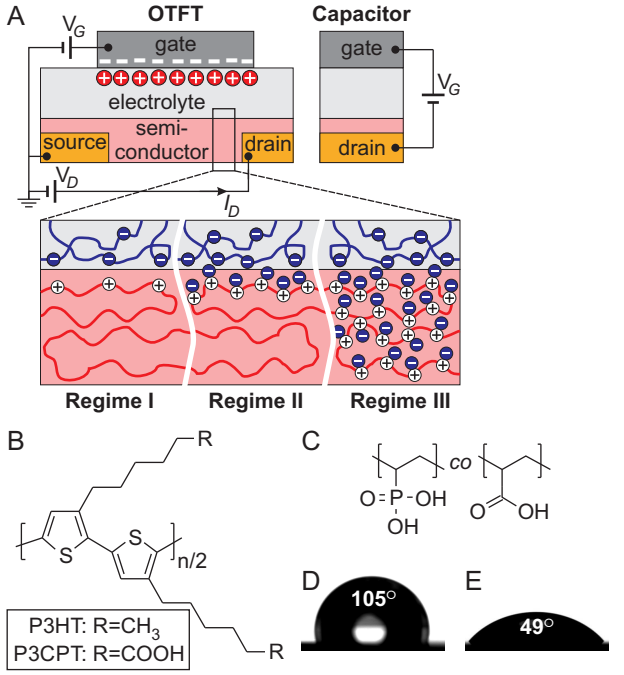

Fig. 1. Device architectures and chemical structures of the materials used in this study. (*A*) Schematic diagram of a capacitor structure and a polyelectrolyte-gated OTFT under a negative gate voltage illustrating three different operational regimes; field-effect (Regime I) and interfacial and bulk electrochemical (Regimes II and III, respectively). The chemical structures of (*B*) regioregular poly(3-hexylthiophene) (P3HT), poly(3-carboxypentylthiophene) (P3CPT) and (*C*) poly(vinylphosphonic acid-*co*-acrylic acid) (P(VPA-AA)). Profiles of water droplets on (*D*) P3HT and (*E*) P3CPT surfaces with contact angle of 105° and 49°, respectively.

constitutes a great problem for fabrication of top-gate/bottom-contact polyelectrolyte-gated OTFTs (Fig. 1*A*) where the hydrophilic polyelectrolyte film needs to be deposited from an aqueous solution on top of the hydrophobic semiconductor surface. Inkjet printing of the polyelectrolyte on top of P3HT has turned out to be very challenging and even spin-coating of the polyelectrolyte is not straightforward. Two different approaches have been explored to reduce the water contact angle and to facilitate spin-coating of the polyelectrolyte on P3HT, namely, use of a surfactant [22] or a binary solvent mixture. [13] However, the better wettability of P3CPT could solve these manufacturing challenges.

Maps of the electrochemical activity. Previously, impedance spectroscopy has been employed to survey polarization mechanisms of electrolytes under an electric field. [23] Here our aim was to use impedance spectroscopy to map the boundary between field-effect and electrochemical regimes in OTFTs. For this purpose thin films of a polyelectrolyte poly(vinylphosphonic acid-*co*-acrylic acid) (P(VPA-AA), Fig. 1*C*) together with either P3CPT or P3HT were sandwiched between Ti and Au electrodes to give capacitor structures (Fig. 1*A*) which were characterized by impedance spectroscopy. In addition to a small AC voltage ($V_{AC,rms} = 0.1$ V), we also applied a DC voltage bias ($V_{DC} = 0 \ldots -1.5 \ldots 0$ V) to the capacitors in order to explore the influence of a gate voltage, V_G, on the impedance characteristics. The phase angle plots (Θ vs. frequency, Fig. 2*A*) can be divided into two parts depending on the value of Θ. Capacitive behavior is predominant when $\Theta < -45°$ whereas resistive behavior dominates when $\Theta > -45°$.

When a low gate voltage was used ($|V_{DC}| < 0.6$ V), the capacitor structures comprising P3CPT (Fig. 2*A*) exhibited resistive behavior at high frequencies (>30 kHz) due to dissociation and migration of protons from the polyelectrolyte chains whereas capacitive behavior was more dominant at lower frequencies (<30 kHz), which can be attributed to the formation of electric double layers along the Ti/P(VPA-AA) and P3CPT/P(VPA-AA) interfaces. [13, 23] As a comparison, the P3HT-based capacitors gave very similar results when $|V_{DC}| < 0.6$ V (see supporting information Fig. S1). However, when the DC bias was increased further ($|V_{DC}| > 0.9$ V), striking differences between P3HT and P3CPT were revealed. In P3CPT-based capacitors, the phase angle showed a significant increase that was accompanied by a simultaneous increase in the effective capacitance, suggesting a second mechanism by which the capacitor becomes more charged at low frequencies (Fig. 2). As an example, at $V_G = -1.5$ V the capacitors showed resistive behavior almost throughout the entire frequency range together with very high capacitance, thus implying that migration of ions dominate in this voltage range. We interpret these results as an indication of electrochemical doping of P3CPT which takes place at high voltages and low frequencies. However, the symmetry in the phase angle and capacitance plots across $V_{DC} = -1.5$ V suggests that the electrochemical doping processes were reversible.

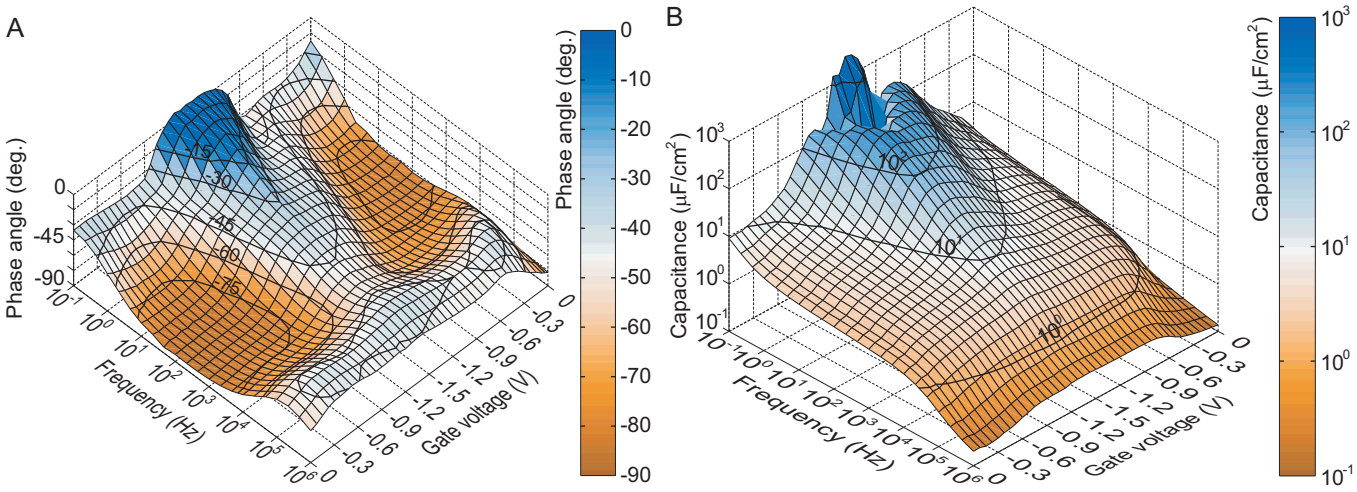

Fig. 2. Phase angle (*A*) and capacitance (*B*) plots as a function of frequency and applied DC bias for a capacitor structure of Au/P3CPT/P(VPA-AA)/Ti. The effective capacitance was calculated from the complex impedance by using an equivalent circuit comprising a resistor and a capacitor in parallel.

Output and transfer characteristics. Next, top-gate/bottom-contact OTFTs were fabricated using a similar sandwiched structure as described above (Fig. 1*A*). Fig. 3 shows typical transfer (drain current I_D vs gate voltage V_G) and output characteristics (I_D vs drain voltage V_D) of the OTFTs comprising P3CPT and P(VPA-AA) semiconductor and polyelectrolyte layers, respectively. Current-voltage characteristics showed negligible hysteresis when the OTFTs were operated at low voltages ($|V_G| < 0.5$ V) which implies that the electric double layers were formed rapidly and which also rules out the possibility of extensive electrochemical doping of the semiconductor bulk (see Fig. 3*A* and *B*). The field-effect mobility was calculated from a $(-I_{D,sat})^{1/2}$ vs V_G plot by fitting a straight line for $V_G < -0.4$ V and using the following equation

$$\mu = \frac{2L}{WC_i}\left(\frac{\partial}{\partial V_G}\sqrt{-I_{D,sat}}\right)^2, \qquad [1]$$

where $C_i = 4$ μF/cm^2 (Fig. 2*B*) is the capacitance per unit area of the gate insulator layer, $W = 1000$ μm and $L = 3$ μm the channel width and length and the last term gives the slope of the fitted line. The resulting mobility is $\mu = 2 \cdot 10^{-4}$ cm^{2}V^{-1}s^{-1}.

The situation was very different at higher gate voltages, $|V_G| > 1.0$ V (see Fig. 3*C* and *D*). As compared to the former regime, a much higher output current, on-off ratio and a high degree of hysteresis were observed. We will refer to these two regimes as Regime I and III (Fig. 1*A*) and will show further evidence that they are represented by a field-effect and an electrochemical mode of operation, respectively.

As a comparison, the electrical characteristics of the well-studied P3HT-based OTFTs [13] showed clear current modulation and negligible hysteresis throughout the studied voltage range (see supporting information Fig. S2), supporting the earlier indications [13] that they operate mainly in the field-effect regime.

Switching transients. The switching characteristics of a transistor can be used as a probe to determine whether the transistor operates in the field-effect or electrochemical regime. More precisely, fast switching speed (<ms) is characteristic for the former regime whereas the switching of electrochemical transistors occurs more slowly (s) and is typically limited by the diffusion rate of ions in and out from the semiconductor film. Fig. 4 shows the source current switching characteristics of P3CPT-based OTFTs at two different gate voltage ranges when the OTFTs were switched on and off (Off→On: $V_G = 0 \rightarrow -0.5/-1.5$ V and On→Off: $V_G = -0.5/-1.5 \rightarrow 0$ V in Fig. 4). A constant voltage and a square-wave voltage was applied to the drain and gate electrode, respectively, while the source current was monitored. A current that arises from the charging of the gate capacitor was removed from the transients by subtracting a response at $V_D = 0$ V from the response at $V_D \neq 0$ V [4]. On and off switching times were defined as the time required to reach 90% and 10% of the on and off state, respectively (see Table 1).

P3CPT-based OTFTs showed fast switching characteristics at low gate voltage ($V_G = V_D = -0.5$ V, Fig. 4*A*), similar to the P3HT-based OTFTs (see supporting information Fig. S3), which suggests that they operate in the field-effect regime (Regime I in Fig. 1*A*). Surprisingly, at high gate voltage ($V_G = V_D = -1.5$ V, Fig. 4*B*) the source current of the P3CPT-based OTFTs first exhibited an intermediate on mode (Regime II), which was followed by a second, relatively slower rise (Regime III). Importantly, the P3CPT-based OTFTs could be continuously operated solely in Regime II without drifting to Regime III provided that the pulse length of the applied gate voltage was limited to less than 100 ms (Fig. S5). The second gradual rise (Regime III) can be attributed to electrochemical doping and charge transport in the *bulk* of P3CPT (Regime III, Fig 1*A*) but further evidence is required to define the origin of the fast response (Regime II).

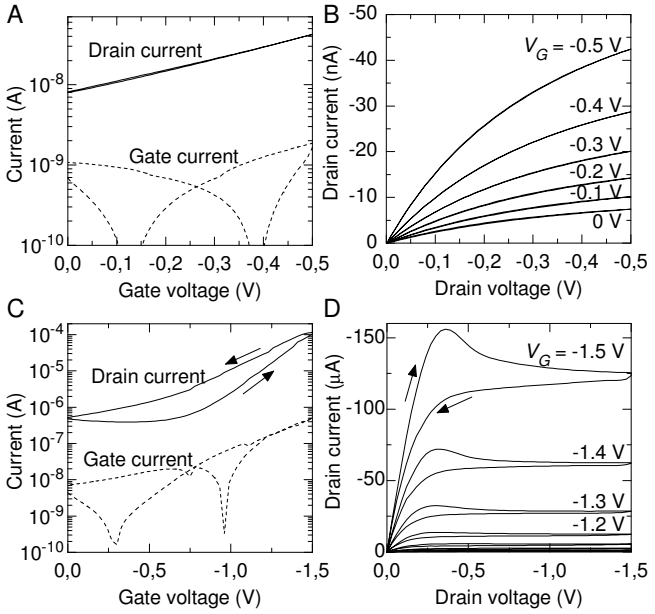

Fig. 3. Electrical characteristics of P3CPT-based OTFTs. (*A*) Transfer and (*B*) output curves under low gate voltage ($V_{G,min} = V_{D,min} = -0.5$ V). (*C*) transfer and (*D*) output curves under high gate voltage ($V_{G,min} = V_{D,min} = -1.5$ V).

Current versus semiconducting layer thickness. It is generally agreed that in a field-effect transistor, the flow of charge carriers from source to drain is confined to the very first monolayers next to gate dielectric. [24,25] This gives that the output current of a field-effect transistor is more or less independent of the semiconductor layer thickness provided that the film morphology remains the same regardless of the thickness. In electrochemical transistors, on the contrary, the output current is expected to scale linearly with the active layer thickness due to that electrochemical doping and charge transport occur throughout the entire bulk of the active layer. [26] Fig. 5 shows the channel current of the transistors as a function of the P3CPT film thickness. Each measurement point is an average over five different transistors, with the error bars indicating the highest and lowest measured current in the five transistors. The current values at low ($V_G = -0.5$ V) and high gate voltage ($V_G = -1.5$) were extracted from the transfer and switching characteristics, respectively. At low gate voltage ($V_G = -0.5$ V), the output current is independent of the P3CPT film thickness, suggesting that, the doping and

Table 1. Switching times of the OTFTs.

			Switching time	
Semiconductor	V_G	Regime*	on	off
P3HT	-0.5 V	**I**	1.9 ms	0.4 ms
P3HT	-1.5 V	**I**	1.7 ms	0.3 ms
P3CPT	-0.5 V	**I**	7.0 ms	2.4 ms
P3CPT	-1.5 V	**II**	9 ms	15 ms†
P3CPT	-1.5 V	**III**	3.4 s	0.3 s

*See Fig. 4, Fig. S3 and Fig. 1*A*.

†Extracted from a switching off curve ($V_G = -1.5 \rightarrow 0$ V) after having been held at $V_G = V_D = -1.5$ V for 50 ms.

charge transport occurs exclusively at the interface of P3CPT rather than in the bulk (Regime I, Fig 1*A*). At high gate voltage ($V_G = -1.5$ V), the transistors showed two different regimes, as was shown in the switching characteristics (Fig. 4*B*). Remarkably, the fast intermediate mode shows no current dependence on the P3CPT film thickness (Regime II, Fig. 5) which implies that the charge transport is confined to a thin layer of the semiconductor, next to the polyelectrolyte interface. Assuming surface transport, we can estimate the sheet conductance $\sigma_{sheet} = \frac{I}{V_D}\frac{L}{W} = 140$ nS sq^{-1}, where $I = 70$ μA is the channel current (Fig. 5), $V_D = -1.5$ V is the drain voltage, $W = 1000$ μm and $L = 3$ μm the channel width and length, respectively. In the subsequent slow Regime III, the output current scales linearly with the P3CPT film thickness (Fig. 5) indicative of electrochemical bulk doping. The bulk conductivity in Regime III can be extracted from Fig. 5 by using $\sigma_{bulk} = \frac{I}{V_D}\frac{L}{Wd}$ where d is the P3CPT film thickness. This gives $\sigma_{bulk} = 0.2 \pm 0.05$ S/cm.

Operation mechanism. Finally, we will discuss the probable operation mechanisms in each of the three observed regimes.

Regime I is characterized by negligible hysteresis (Fig. 3*A* and *B*), fast switching speed (Fig. 4*A*) and thickness-independent channel current (Fig. 5). These different lines of evidence all point to purely field-induced gating i.e. field-effect mode of operation. Here, the P(VPA-AA) polyanions alone balance the polarons in the semiconductor similar to the polyelectrolyte gated P3HT-based transistors [13].

Regime III is characterized by high current density (10^3 A/cm^2), large hysteresis in the electrical characteristics (Fig. 3*C* and *D*), slow switching speed (Fig. 4*B*) and a channel current linearly increasing with the semiconductor film thickness (Fig. 5). Moreover, the switching times of the P3CPT-based OTFTs increased with increasing P3CPT layer thickness (see supporting information Fig S4). This is clear evidence that Regime III corresponds to electrochemical doping in the *bulk* of P3CPT and consequent 3D charge transport, with bulk conductivity of 0.2 S/cm.

Regime II is characterized by high current levels, fast switching speed (Fig. 4*B* and Fig. S5) and thickness-independent channel current (Fig. 5). Despite the fast switching speed, we deduce that electrochemical doping process governs the operation of the OTFTs in Regime II as well because of an exceptionally high current level ($I_D > 50\mu$A). We can estimate the typical doping depth in Regime II by fitting two lines through the data points of Regime II and III in Fig. 5. It turns out that the lines cross at a film thickness of 1.5-8.4 nm which correspond to a thickness of one to five monolayers [18]. Assuming surface charge transport, we can estimate the mobility in Regime II by using $I_{sat} = \frac{W}{2L}\mu C_i(V_G - V_T)^2$, where $I_{sat} = 70$ μA (Fig. 5), $C_i = 70$ μF/cm^2 (Fig. 2*B*), $V_G = -1.5$ V and $V_T = 0$ V is the threshold voltage. This gives $\mu = 2.7 \cdot 10^{-3}$ cm^{2}V^{-1}s^{-1}. The higher mobility in Regime II, as compared to Regime I can be attributed to higher charge carrier density. [27] In conclusion, charge carriers in Regime II are confined to a few monolayers close to the polyelectrolyte/semiconductor interface, giving rise to a high current density (10^3 A/cm^2).

A question arises as to the origin of the electrochemical Regimes II and III. Electrochemical doping of a semiconductor in an electrolyte gated transistor typically involves migration of small ions from the electrolyte into the semiconductor bulk. [7] In the present OTFTs, however, the anions of the P(VPA-AA) are immobile due to the covalent binding to the polymer backbone which is expected to significantly suppress electrochemical bulk doping. Indeed, all the results presented here indicate that electrochemical bulk doping does not occur in the P3HT-based OTFTs under the studied voltage range. However, each repeat unit of the P3CPT bears an additional carboxyl side group. Impedance spectroscopy showed evidence that the protons of the carboxyl groups of P3CPT start to dissociate and migrate towards the bulk of P(VPA-AA) when the gate voltage is high enough ($|V_G| > 0.9$ V). The remaining carboxylate anions are suggested to balance the positive polarons in the P3CPT backbone. This self-doping of the conjugated P3CPT backbone by the anionic carboxylate side groups is proposed to serve as the driving force for the electrochemical doping in Regimes II and III under high gate voltage. The protons in the first monolayers of P3CPT have only a little energy barrier to migrate to the P(VPA-AA) layer whereas in the bulk of P3CPT, the alkyl side chains of P3CPT create a higher energy barrier to the passage of protons. Therefore, Regime II is assigned to a *fast* process associated with the transport of protons from a few monolayers of P3CPT to the P(VPA-AA) whereas Regime III is assigned to a *slow* process associated with the transport of protons in the P3CPT bulk.

What remains to be identified is the type of the process at the gate electrode/polyelectrolyte interface. There are two options [28]; the electrochemical doping of P3CPT is balanced by charging of an ionic double layer at the gate electrode and/or by an electrochemical half-reaction that takes place at the gate via, e.g., reduction of protons to dihydrogen gas. We believe that the former option is more probable based on the high capacitance of the electric double layer at the gate (Fig. 2) and the reversibility in the electrical characteristics (see supporting information, *Process at the gate electrode*).

Conclusions. We have fabricated polyelectrolyte-gated organic thin-film transistors (OTFTs) comprising a semiconducting layer of carboxyl-functionalized polyalkylthiophenes, and we have shown

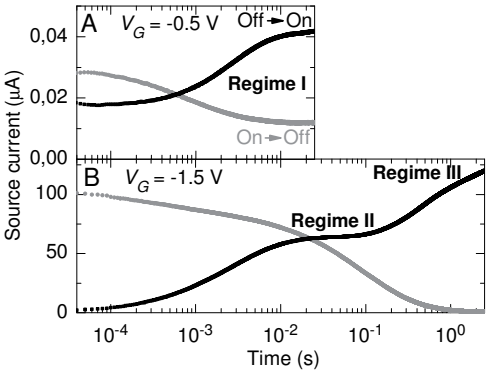

Fig. 4. Switching characteristics of P3CPT-based OTFTs under (*A*) low gate voltage ($V_D = V_G = -0.5$ V) and (*B*) high gate voltage ($V_D = V_G = -1.5$ V).

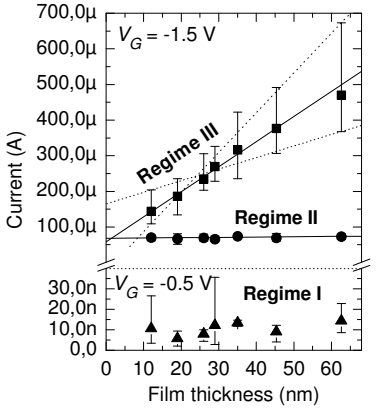

Fig. 5. Channel current as a function of P3CPT film thickness at low gate voltage (triangles) in Regime I and at high gate voltage in Regime II (circles) and in Regime III (squares). Each measurement point is an average over five different transistors, with the error bars indicating the highest and lowest measured current in the five transistors.

that the OTFTs can be operated in three different regimes. At low gate bias, the OTFTs operate similar to a conventional field-effect transistor (Regime I). At high gate bias, electrochemical doping dominates and the extent of doping can be controlled by the duration of the applied gate bias; a fast intermediate regime is characterized by charge transport through a few monolayers (Regime II) and a slow regime by 3D charge transport through the bulk of the semiconductor (Regime III). Regime II is especially interesting because of the low operating voltage, high current density (10^3 A/cm^2) and fast switching speed (10^{-2} s). Furthermore, we have proposed a design methodology to build digital circuits comprising P3CPT-based transistors that operate only in Regime II (supporting information). These circuits can find applications in printed electronic systems where e.g. control of a display cell is done using OTFTs that operate in Regime II. The superior wettability of the conjugated polyelectrolyte surface toward aqueous solutions could pave the way for printing of the polyelectrolyte-gated OTFTs. Finally, the carboxyl group of the conjugated polyelectrolyte can be used to immobilize various biomolecules, which could allow construction of various biosensors where the covalent linkage between the biomolecule and the carboxyl groups of the sensor would trigger a significant change in the conductivity of the transistor. [29] Finally, the results presented here provide guidelines for designing enhancement-mode electrochemical transistors that do not only carry high current densities but can also switch fast.

Materials and Methods

Materials. Regioregular poly(3-hexylthiophene) (P3HT) and poly(3-carboxypentylthiophene) (P3CPT) were purchased from Sigma-Aldrich and Rieke Metals Inc., respectively, and were used without further purification. Poly(vinylphosphonic acid-*co*-acrylic acid) (P(VPA-AA)) was obtained from Rhodia.

Device fabrication. Top-gate/bottom-contact OTFTs were fabricated as follows. First, an adhesive 5-nm-thick chromium layer and a 50-nm-thick gold layer were thermally evaporated onto borosilicate glass substrates. Standard photolithography and wet-etching were used to pattern interdigitated source and drain electrodes onto the glass substrates. P3CPT and P3HT were dissolved in analytical grade dimethyl sulfoxide (5-20 mg/ml) and 1,2-dichlorobenzene (10 mg/ml), respectively, sonicated at 60°C for 10 min and finally passed through 0.2 μm Nylon and PTFE filters, respectively. The warm solutions (60°C) were spin coated on pre-heated substrates (105-110°C) and the resulting semiconductor thin films were dried in a vacuum oven at 110°C for 2 min. The thickness of the P3CPT film (12 to 63 nm) was controlled by varying the concentration of P3CPT in dimethyl sulfoxide (5 and 20 mg/ml) and the spin-coating speed (1500 to 4000 rpm). The thickness of the semiconductor film was 30 nm if not otherwise stated. P(VPA-AA) polyelectrolyte was dissolved (20 mg/ml) in a mixture of 1-propanol and deionized water (4:1 vol:vol), passed through a 0.2 μm Nylon filter, spin-coated onto the semiconductor film at 3000 rpm for 60 s and finally dried in a vacuum oven at 110°C for 2 min. Typical film thickness of the polyelectrolyte was 53-57 nm. Devices were completed by thermally evaporating Ti gate electrodes through a nickel shadow mask. All the transistors had the same channel length ($L = 3$ μm) and width ($W = 1000$ μm).

Characterization. Contact angle measurements were carried out on a CAM 200 contact angle meter (KSV Instruments) and the photographs of the water droplets (7 μL) were analyzed by Attension Theta software (Biolin Scientific). Film thicknesses were measured by using an ellipsometer (Sentech SE400) and a surface profilometer (Veeco, Dektak 3 ST). The impedance data were collected with an alpha high-resolution dielectric analyzer (Novocontrol GmbH) by scanning from 1 MHz to 0.1 Hz while applying an rms amplitude of 0.1 V and a constant DC voltage to a Ti-electrolyte-semiconductor-Au capacitor (100 μm $\times$ 100 μm). Output and transfer characteristics were measured with a Keithley semiconductor characterization system (4200-SCS) at a scan rate of 0.2 V/s. The switching transients were obtained with an oscilloscope (Agilent 54832D Infiniium) by measuring a voltage drop across a resistor connecting the source electrode to ground while applying a square wave voltage to the gate electrode (Agilent 33120A waveform generator) and a DC voltage to the drain electrode (Agilent E3631A power supply). A parasitic current that arises from charging of the gate capacitor was removed from the transients by subtracting a response measured at $V_D = 0$ V from the response measured at $V_D \neq 0$ V [4]. Current versus film thickness measurements were carried out on the same systems as the switching transients and the output/transfer characteristics. The current values at low gate voltage (at $V_G = V_D = -0.5$ V) were extracted from the transfer characteristics whereas at higher gate voltage ($V_G = V_D = -1.5$), the transistors were biased until the saturation of the drain current. In both cases, the off current (at $V_G = 0$ V and $V_D = -0.5$ or -1.5 V) was subtracted from the on current to eliminate effects arising from a leakage current between source and drain. All measurements were carried out in ambient conditions at room temperature (40% relative humidity).

ACKNOWLEDGMENTS. The authors wish to thank The Swedish Government (the Advanced Functional Materials project), the Swedish Foundation for Strategic Research (the OPEN project) and the Knut and Alice Wallenberg Foundation for financial funding of this project. This work was also partially supported by the EU through the EC FP7 ONE-P large-scale project (no. 212311). A.L. thanks the Finnish Academy (project 135737) and the Foundation of Technology, Finland for financial support. M.B. wishes to thank the Önnesjö Foundation for financial support. Prof. Olle Inganäs, Dr. Isak Engquist (both from Linköping University), Dr. Peter Andersson Ersman and Dr. Mats Sandberg (both from Acreo AB) are gratefully acknowledged for fruitful discussions.

1. **Reuss RH, et al. (2005) Macroelectronics: Perspectives on technology and applications. *Proc IEEE* 93:1239–1256.**
2. **Sirringhaus H, Kawase T, Friend RH, Shimoda T, Inbasekaran M, Wu W, Woo EP (2000) High-resolution inkjet printing of all-polymer transistor circuits. *Science* 290:2123–2126.**
3. **Cho JH, Lee J, He Y, Kim B, Lodge TP, Frisbie CD (2008) High-capacitance ion gel gate dielectrics with faster polarization response times for organic thin film transistors. *Adv Mater* 20:686–690.**
4. **Herlogsson L, Noh YY, Zhao N, Crispin X, Sirringhaus H, Berggren M (2008) Downscaling of organic field-effect transistors with a polyelectrolyte gate insulator. *Adv Mater* 20:4708–4713.**
5. **Ono S, Seki S, Hirahara R, Tominari Y, Takeya J (2008) High-mobility, low-power, and fast-switching organic field-effect transistors with ionic liquids. *Appl Phys Lett* 92:103313–103315.**
6. **Dhoot AS, Yuen JD, Heeney M, McCulloch I, Moses D, Heeger, AJ 2006 Beyond the metal-insulator transition in polymer electrolyte gated polymer field-effect transistors. *Proc Natl Acad Sci* USA 103:11834–11837.**
7. **Yuen JD, Dhoot AS, Namdas EB, Coates NE, Heeney M, McCulloch I, Moses D, Heeger AJ (2007) Electrochemical doping in electrolyte-gated polymer transistors. *J Am Chem Soc* 129:14367–14371.**
8. **Mills T, Kaake LG, Zhu XY (2009) Polaron and ion diffusion in a poly(3-hexylthiophene) thin-film transistor gated with polymer electrolyte dielectric. *Appl Phys A-Mater Sci Process* 95: 291–296.**
9. **Panzer MJ, Frisbie CD (2007) Polymer electrolyte-gated organic field-effect transistors: Low-voltage, high-current switches for organic electronics and testbeds for probing electrical transport at high charge carrier density. *J Am Chem Soc* 129:6599–6607.**
10. **Kaihovirta N, Aarnio H, Wikman CJ, Wilen CE, Österbacka R (2010) The effects of moisture in low-voltage organic field-effect transistors gated with a hydrous solid electrolyte. *Adv Funct Mater* 20:2605–2610.**
11. **Kergoat L, Herlogsson L, Braga D, Piro B, Pham MC, Crispin X, Berggren M, Horowitz G (2010) A water-gate organic field-effect transistor. *Adv Mater* 22:2565–2569.**
12. **Shimotani H, Diguet G, Iwasa Y (2005) Direct comparison of field-effect and electrochemical doping in regioregular poly(3-hexylthiophene). *Appl Phys Lett* 86:022104–022106.**
13. **Herlogsson L, Crispin X, Robinson ND, Sandberg M, Hagel OJ, Gustafsson G, Berggren M (2007) Low-voltage polymer field-effect transistors gated via a proton conductor. *Adv Mater* 19:97–101.**
14. **Panzer MJ Frisbie CD (2006) High carrier density and metallic conductivity in poly(3-hexylthiophene) achieved by electrostatic charge injection. *Adv Funct Mater* 16:1051–1056.**
15. **Andersson P, Nilsson D, Svensson PO, Chen MX, Malmstrom A, Remonen T, Kugler T, Berggren M (2002) Active matrix displays based on all-organic electrochemical smart pixels printed on paper. *Adv Mater* 14:1460–1464.**
16. **Andersson P, Forchheimer R, Tehrani P, Berggren M (2007) Printable all-organic electrochromic active-matrix displays. *Adv Funct Mater* 17:3074–3082.**
17. **Duarte A, Pu KY, Liu B, Bazan GC (2011) Recent advances in conjugated polyelectrolytes for emerging optoelectronic applications. *Chem Mater* 23:501–515.**
18. **Worfolk BJ, Rider DA, Elias AL, Thomas M, Harris KD, Buriak JM (2011) Bulk Heterojunction Organic Photovoltaics Based on Carboxylated Polythiophenes and PCBM on Glass and Plastic Substrates. *Adv Funct Mater* 21: 1816–1826.**
19. **Lan LF, Xu RX, Peng JB, Sun ML, Zhu XH, Cao Y (2009) Dipole-induced organic field-effect transistor gated by conjugated polyelectrolyte. *Jpn J Appl Phys* 48:080206–080208.**

20. Ding L, Jonforsen M, Roman LS, Andersson MR, Inganas O (2000) Photovoltaic cells with a conjugated polyelectrolyte. *Synth Met* 110:133–140.
21. Bao ZN Lovinger AJ (1999) Soluble regioregular polythiophene derivatives as semiconducting materials for field-effect transistors. *Chem Mater* 11:2607–2612.
22. Said E, Crispin X, Herlogsson L, Elhag S, Robinson ND, Berggren M (2006) Polymer field-effect transistor gated via a poly(styrenesulfonic acid) thin film. *Appl Phys Lett* 89:143507–143509.
23. Larsson O, Said E, Berggren M, Crispin X (2009) Insulator polarization mechanisms in polyelectrolyte-gated organic field-effect transistors. *Adv Funct Mater* 19:3334–3341.
24. Dodabalapur A, Torsi L, Katz HE (1995) Organic transistors - 2-dimensional transport and improved electrical characteristics. *Science* 268:270–271.
25. Tanase C, Meijer EJ, Blom P. WM, de Leeuw DM (2003) Local charge carrier mobility in disordered organic field-effect transistors. *Org Electron* 4:33–37.
26. Bernards DA, Malliaras GG (2007) Steady-state and transient behavior of organic electrochemical transistors. *Adv Funct Mater* 17:3538–3544.
27. Arkhipov VI, Emelianova EV, Heremans P, Bassler H (2005) Analytic model of carrier mobility in doped disordered organic semiconductors *Phys Rev B* 72:235202–235206.
28. Lin FD, Lonergan MC (2006) Gate electrode processes in an electrolyte-gated transistor: Non-faradaically versus faradaically coupled conductivity modulation of a polyacetylene ionomer. *Appl Phys Lett* 88:133507–133509.
29. Cosnier S (1999) Biomolecule immobilization on electrode surfaces by entrapment or attachment to electrochemically polymerized films. a review. *Biosens Bioelectron* 14:443–456.

Supporting Information

Laiho et al.
www.pnas.org/cgi/doi/10.1073/pnas.1107063108

SI Text

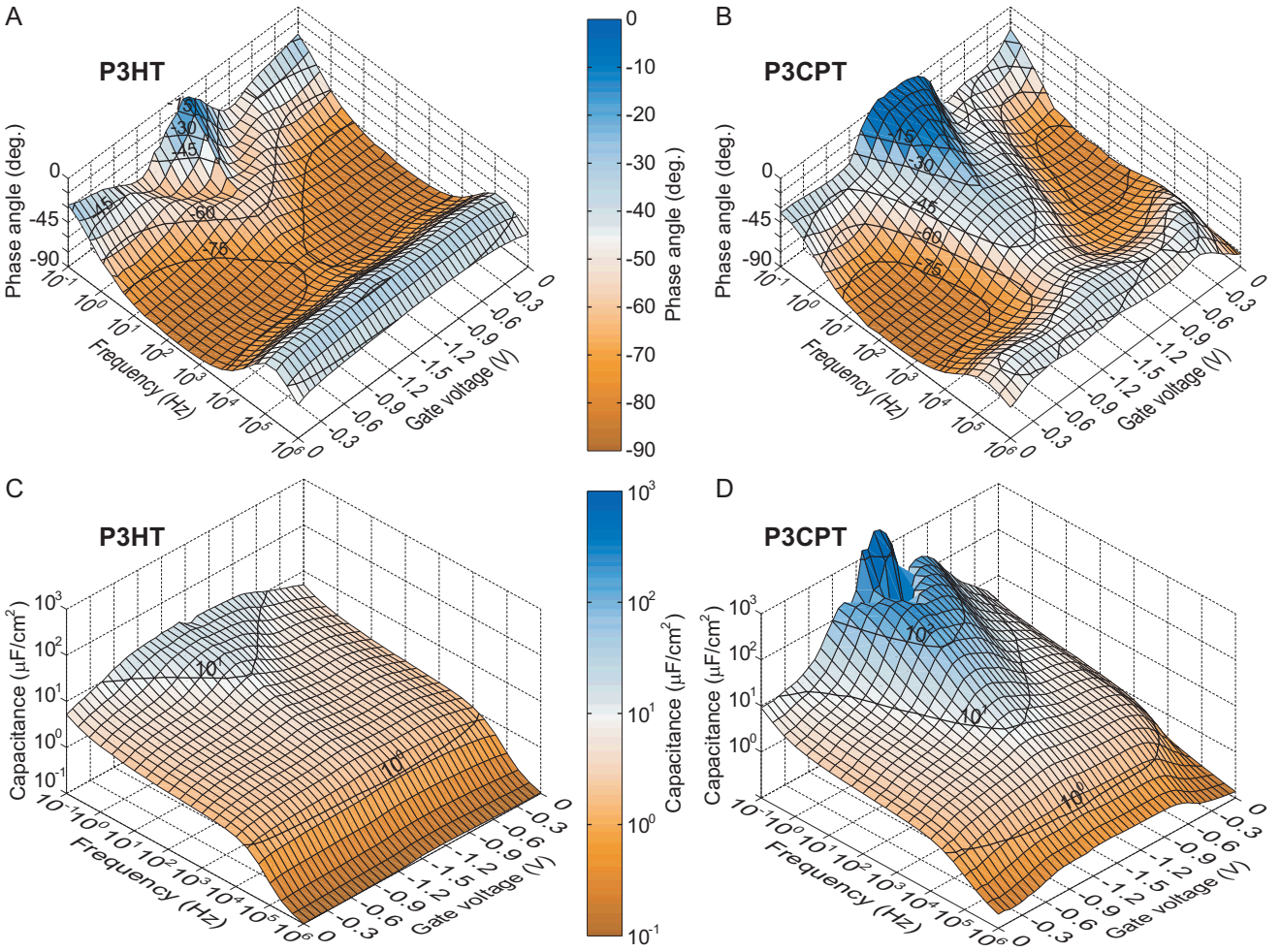

Fig. 1. Comparison of the phase and capacitance plots of P3CPT and P3HT-based capacitors. Phase angle plots as a function of frequency and applied DC bias for a capacitor structure of (*A*) Au/P3HT/P(VPA-AA)/Ti and (*B*) Au/P3CPT/P(VPA-AA)/Ti. Effective capacitance as a function of frequency and applied DC bias for a capacitor structure of (*C*) Au/P3HT/P(VPA-AA)/Ti and (*D*) Au/P3CPT/P(VPA-AA)/Ti. The effective capacitance was calculated from the complex impedance by using an equivalent circuit comprising a resistor and a capacitor in parallel.

Publication footnotes

Switching transients

The switching times of the reference P3HT-based OTFT are nearly identical in the low and high voltage range (Fig. S3*A* and *B*, respectively). Moreover, after being switched on for 1 ms, the channel current shows only a small increase (Fig. S3*B*) that is attributed to the refinement of the electric double layers as was evidenced in the capacitance plots (Fig. 1*C*). The fast switching speeds and the absence of significant current increase at longer time scales suggests that the P3HT-based OTFTs operate in the field-effect regime (Regime I).

Process at the gate electrode

There are two options for the process at the gate electrode/polyelectrolyte interface[1]; the electrochemical doping of P3CPT is balanced by charging of an ionic double layer at the gate electrode and/or by an electrochemical half-reaction that takes place at the gate via, e.g., reduction of protons to dihydrogen gas. We believe that the former option is more probable in the present case. Our reasoning is as follows.

We can estimate that one polaron occupies a volume of roughly $V_p = 1200$ Å^3 by using the X-ray diffraction data[2] and by assuming that one polaron occupies five monomer units.[3] A fully doped P3CPT channel corresponds to $N_p = V_p^{-1} WLd$ polaronic transport states, where $W = 1$ mm and $L = 3$ μm are the width and length of the channel, respectively, and $d = 63$ nm is the P3CPT film thickness. This number of charges needs to be compensated by the electric double layer at the gate which gives that the gate capacitance must be at least $C_{min} = \frac{eN_p}{|V_G|A_G} = 4$ μF/cm^2 where e is the unit charge, $V_G = -1.5$ V the gate voltage and $A_G = 600 \times 700$ μm^2 the area of the gate electrode. This capacitance value (4 μF/cm^2) is far below the measured values for P3CPT-based capacitors (Fig. S1*D*) suggesting that the electric double layer at the gate electrode can compensate for the charges in the P3CPT film.

Stable operation in Regime II

To test whether the transistors can be stabilized and operated over long time scales in Regime II, we performed long-time transient measurements where we applied different square wave voltages to the gate electrode, held the drain electrode at constant potential and measured the source current. Fig. S5*C* shows that during 1000 sequential ON/OFF cycles (10 ms ON and 10 ms OFF) the switching times and the current levels of the OTFTs remain virtually constant. This is clear evidence that the transistor has remained in Regime II and has not drifted to Regime III. When the duration of the ON time was increased from 10 ms to 100 ms, the time required to switch the transistor back to the OFF state increased remarkably (Fig. S5*D*). Even if the transistors seemed to drift to Regime III during the 100 ms ON time (Fig. S5*D*), the following 100 ms OFF time was sufficient to return the transistor back to Regime II as evidenced by the fast and constant switch ON time. In conclusion, the transistors can be stabilized and operated in Regime II if the duration of the ON time is set to 100 ms or less and the time between successive ON states is as long as the total ON time.

The temporal confinement of the charge transport to a thin layer of the semiconductor (as described above) offers one way to stabilize the transistor in the interfacial doping regime (Regime II). However, spatial confinement of the electrochemical doping may allow a second method. As shown in Fig. 5, the Regimes II and III may merge when the semiconductor film is only a couple of monolayers thick. This merger is also supported by the fact that the switching times decrease with decreasing film thickness in Regime III (Fig. S4). Moreover, the semiconducting P3CPT could be cross-linked at its carboxyl groups by using e.g. ethylene glycol which could lead to deactivation of Regime III. Also, improvement of the semiconducting polymer morphology could suppress Regime III.

Electrochromic polymers, whose oxidation state determines their optical absorption characteristics, can be used to fabricate electrochromic displays for electronic paper technology.[4, 5] In order to switch such a display, a relatively large amount of charge needs to be transferred to/from the display, and therefore electrochromic displays are often driven by electrochemical transistors. As an example, operation of an electrochromic pixel of the size of 1 mm^2 requires that a total charge of approximately 5 μC is transferred to/from the display every time the pixel is switched.[5] If we integrate the transient response of the P3CPT-based transistor (Fig. S5*D*), we get that during one 100 ms ON cycle a total charge of approximately 7 μC is being transferred which is enough to switch the electrochromic pixel. Current electrochromic active-matrix displays typically comprise *depletion-mode* electrochemical transistors, meaning that a non-zero gate potential is required to keep the transistor in the OFF-state which subjects substantial stress on the transistors.[4, 5] However, if the pixels were driven by the P3CPT-based *enhancement-mode* electrochemical transistors, the transistors would be stressed only when the pixel is being updated (for less than 100 ms) - maintaining the pixel in one state would not require any gate potential on the transistor. Therefore, changing from the depletion-mode to the enhancement-mode transistors would be of particular advantage to printed electronic systems such as electrochromic active-matrix displays. In conclusion, the P3CPT based transistors, operated in Regime II, could be used to drive an electrochromic display.

Design of digital systems working in Regime II.

P3CPT-based transistors can be operated solely in Regime II if the negative gate voltage is applied for a shorter time than 100 ms. The lower limit for the pulse length of the applied gate voltage is roughly 1 ms which still gives a reasonable output current (Fig. S3*D* and Fig. S5*D*). These constraints are different from what is normally the case with traditional transistors and forces a different way to design digital systems. Such systems can be divided into *combinational* and *sequential circuits*. Below, we discuss each of these types and propose how they can be implemented under the described constraints.

Design methodology. The proposal is based on the idea that logical symbols are not represented by voltage levels but instead by the occurrence of a negative-valued pulse (logical 1) and a zero or positive-valued pulse (logical 0) at predetermined time instances. These pulses are shaped such that they can be applied directly to a gate of the P3CPT-based transistor without causing electrochemical bulk doping. When no pulse is applied, a positive idle value is kept on the gate electrode (Fig. S6*A*).

Combinational circuits. Combinational circuits are characterized in that they are "memoryless", i.e. the output is only a function of the current input values and independent on any previous input data. Usually, the implementation of combinational circuits is based on several layers of simpler combinational circuits such as 2-input gates, inverters et cetera. Since only the input signals are pulsed it is not possible to use such a design methodology in this case. Fortunately, a single layer network of serial/parallel transistors can implement most practical combinational networks. This makes it possible to use exactly the same network for pulsed signals as for traditional signals with the only exception that the output has to be converted to a pulsed signal as well. This is illustrated in Fig. S6*B*, which shows how a series transistor is used to obtain the desired output. The 2-input NAND gate shown in Fig. S6*C* exemplifies this design methodology. The output resistor should have a much higher value than the drain resistor.

Sequential circuits. Sequential circuits are characterized by their memory property. This means that the output of such a circuit depends not only on the current input values but also on previous input (or output) values. Principally, any (clocked) sequential circuit

can be implemented as a combinational circuit with feedback and with a (one-cycle) delay in the feedback loop (Fig. S7*A*). Since the *C* circuit can be implemented it remains to find out how to implement the one-cycle delay without violating the transistor constraints. As all the transistors are switched off between the pulses, the state of the circuit has to be kept in some way. Storing the state value in capacitors, a technique that is commonly used in dynamic memories, can solve this. Thus, one proposal for the D circuit is given in Fig. S7*B*.

Pulse generation. The design is not complete unless it is shown that the pulses according to the above criteria can be generated. Here, we discuss two different approaches. (1) *An astable multivibrator* is a classical oscillator. Consisting of only two transistors, four resistors and two capacitors it can be designed to produce pulses of various duration and frequency. However, since neither transistor is allowed to be turned on for a substantial time period it is reasonable that the oscillator is designed for a 50% duty cycle. The odd and even pulses used in the delay circuit are then available from the two transistors, respectively. (2) *A ring oscillator* can be used to produce pulses with 50% duty cycle. Even and odd pulses are available from two consecutive stages in the ring. The short overlap between these pulses needs to be taken into account when designing sequential circuits.

In summary, we have proposed a design methodology to build digital circuits using P3CPT-based transistors running in Regime II. Design principles need to be changed compared to conventional logic design. In particular, instead of static representation of 0:s and 1:s, voltage pulses are used and memory states are stored dynamically in capacitors. Additional components are necessary such as series transistors to provide three-state outputs. Three voltage levels are needed leading to the requirement of two power supplies. These levels correspond to the negative pulse value, the positive pulse value and ground. These circuits can find applications in printed electronic systems where e.g. control of a display cell is done using OTFTs that operate only in Regime II.

1. **Lin FD, Lonergan MC (2006) Gate electrode processes in an electrolyte-gated transistor: Non-faradaically versus faradaically coupled conductivity modulation of a polyacetylene ionomer. *Appl Phys Lett* 88:133507–133509.**

2. **Worfolk BJ, Rider DA, Elias AL, Thomas M, Harris KD, Buriak JM (2011) Bulk Heterojunction Organic Photovoltaics Based on Carboxylated Polythiophenes and PCBM on Glass and Plastic Substrates. *Adv Funct Mater* 21: 1816-1826.**

3. **Westerling M, Österbacka R, Stubb H (2002) Recombination of long-lived photoexcitations in regioregular polyalkylthiophenes. *Phys Rev B* 66:165220–165226.**

4. **Andersson P, Nilsson D, Svensson PO, Chen MX, Malmström A, Remonen T, Kugler T, Berggren M (2002) Active matrix displays based on all-organic electrochemical smart pixels printed on paper. *Adv Mater* 14:1460–1464.**

5. **Andersson P, Forchheimer R, Tehrani P, Berggren M (2007) Printable all-organic electrochromic active-matrix displays. *Adv Funct Mater* 17:3074–3082.**

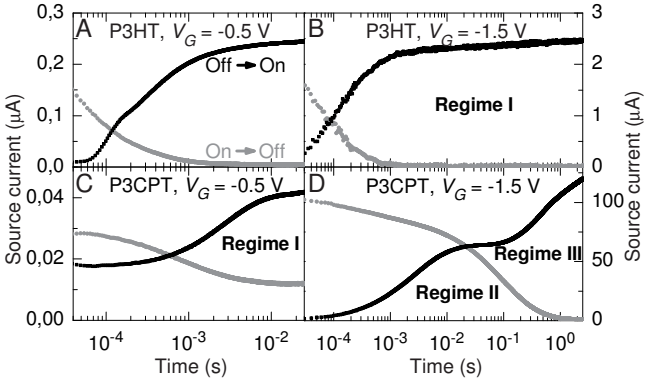

Fig. 3. Switching characteristics of P3HT and P3CPT-based OTFTs. P3HT based OTFT at (*A*) low gate voltage ($V_D = V_G = -0.5$ V) and (*B*) high gate voltage ($V_D = V_G = -1.5$ V). P3CPT based OTFT at (*C*) low gate voltage ($V_D = V_G = -0.5$ V) and (*D*) high gate voltage ($V_D = V_G = -1.5$ V).

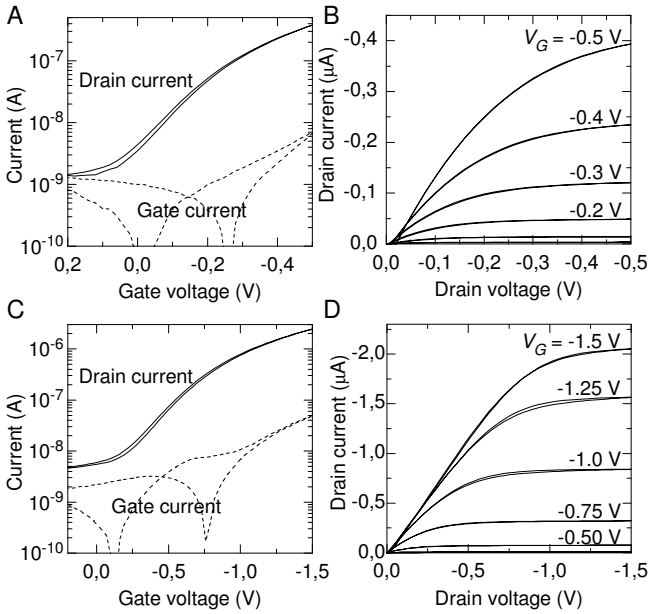

Fig. 2. Electrical characteristics of P3HT-based OTFTs. (*A*) Transfer and (*B*) output curves under low gate voltage ($V_{G,min} = V_{D,min} = -0.5$ V). (*C*) Transfer and (*D*) output curves under high gate voltage ($V_{G,min} = V_{D,min} = -1.5$ V).

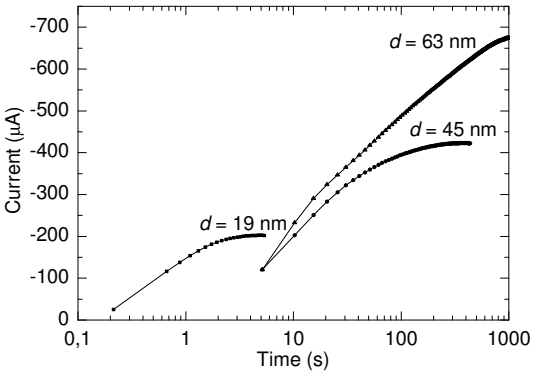

Fig. 4. Switching characteristics of three different P3CPT-based OTFTs with different P3CPT layer thicknesses (19, 45 and 63 nm) in Regime III. Output current and switching times increase with increasing P3CPT layer thickness under high gate voltage ($V_G = V_D = -1.5$ V) in Regime III.

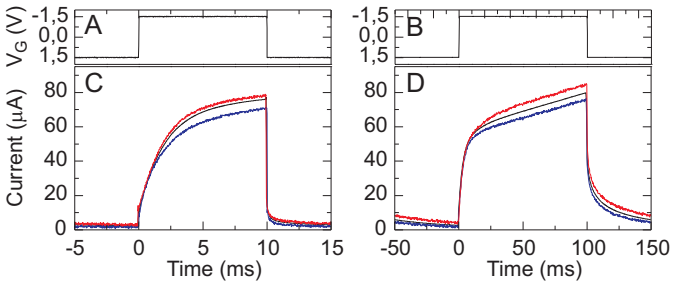

Fig. 5. Switching characteristics of P3CPT-based OTFTs in Regime II. (*A* and *B*) Square wave voltage was applied to the gate electrode (1000 cycles) while the drain electrode was held at $V_D = -1.5$ V. (*C* and *D*) The black curve shows the average source current over the 1000 cycles whereas the blue and the red curves, respectively, show the lowest and the highest source current over the 1000 cycles.

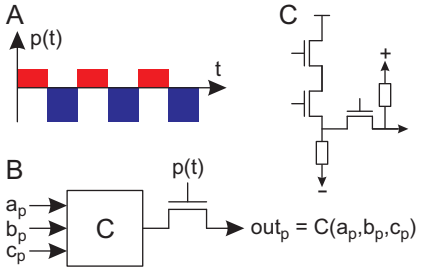

Fig. 6. Design of combinational circuits. (*A*) A basic pulse train with negative pulses interleaved with a positive idle value. (*B*) A modified combinational circuit to work with pulsed signals. (*C*) A 2-input NAND gate with output transistor and resistor to yield positive levels between the logic pulses.

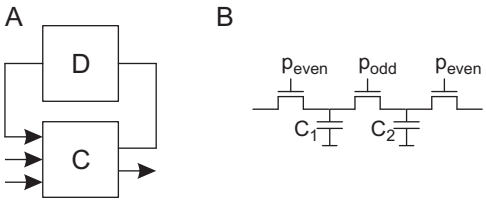

Fig. 7. Design of sequential circuits. (*A*) Example of a sequential circuit where D equals a one-cycle delay. (*B*) Clocked delay circuit where p_{even} and p_{odd} are alternating, non-overlapping pulses, and capacitor C_1 is much larger than C_2.